Generation and Characterization of Multilayer Systems Consisting of $Au_{55}(PPh_3)_{12}Cl_6$ Double Layers and SiO_2 Barrier Films

Torsten Reuter,[a] Stefan Neumeier,[a] Günter Schmid,*[a] Eva Koplin,[b] and Ulrich Simon[b]

Keywords: Gold / Multilayers / Impedance spectroscopy / Bénard–Marangoni effect / Crystallisation

Multilayer systems, consisting of $Au_{55}(PPh_3)_{12}Cl_6$ double layers and SiO_2 barrier films of different thickness, have been generated and characterised. The formation of the double layer between the barrier films was carried out by using spin-coating techniques. For the generation of the SiO_2 films, a plasma-assisted physical vapour deposition (PAPVD) procedure has been applied, based on an anodic plasma arc process. Samples of up to nine cluster/SiO_2 combinations have been produced and have been characterised by AFM and SEM. Impedance measurements showed that there is a characteristic thermally activated frequency dependence of the capacitance of the different systems. The cluster layers interact by dipoles formed in the double layers at low frequencies. It has also been shown that multilayer systems with SiO_2 films thicker than 15 nm tend to spontaneously crystallise. Furthermore, wetting problems during the spin-coating processes have been investigated.

Introduction

Au_{55} clusters, although known for almost 25 years,[1] are still the focus of intensive research, mainly because of their extraordinary electronic properties. The density of states in the valence and in the conduction bands is, compared with that in a bulk piece of metal, dramatically decreased with the result that a metal particle with an extremely small size of 1.4 nm follows quantum mechanical rules instead of the classical laws valid for a bulk metal with an infinitely large number of atoms. Indeed, it has been previously shown that Au_{55} clusters behave as quantum dots that have discrete electronic energy levels.[2,3] Au_{55} clusters act as switches that can be charged and discharged by single electrons, even at room temperature. It is important to mention that individual Au_{55} clusters do not exist in the bare form, and in all cases have to be protected by a shell of appropriate ligand molecules. The nature of such ligand molecules can vary from totally apolar to ionic, with a corresponding change in the solvents in which they are soluble from nonpolar media like alkanes to very polar media like water.[4,5] The existence of a ligand shell is not only necessary for synthetic reasons, but also for prevention of coalescence between bare particles and, last but not least, for profiting from the special electronic properties.

[a] Universität Duisburg Essen,
Universitätsstrasse 5–7, 45117 Essen, Germany
E-mail: guenter.schmid@uni-essen.de
[b] RWTH Aachen,
Landoltweg 1, 52074 Aachen, Germany
E-mail: ulrich.simon@ac.rwth-aachen.de

Our knowledge of the unique electronic properties of Au_{55} clusters prompted us already years ago to look for routes to two-dimensional (2D) organisations, an indispensable condition for the application of these quantum dots in nanoelectronic devices. Perfectly organised monolayers have been generated with limited extension by self-assembly.[6,7] More extended 2D arrangements could be prepared by using chemically modified surfaces[8] or by Langmuir–Blodgett techniques,[9] however, without giving ordered arrays. Artificial structures became available for the first time by using an AFM tip to electrochemically modify pre-prepared surfaces on the nanometre scale.[10] If the order of the clusters is not important, a very simple but effective method can be used. This is the spin coating of dilute solutions of ligand-modified Au_{55} clusters on appropriate surfaces. This technique has been used in the experiments described in this contribution. Spin coating indeed allows to reproducibly generate cluster double layers and, if necessary, monolayers, if the experimental conditions are carefully worked out. Here we report on the generation and on the electric properties of cluster double layers embedded between SiO_2 films of varying thickness. The reason for this research was to find out if thin cluster films, separated from each other by an insulating material, can still communicate with each other, perpendicular to the film plane. From former experiments we know that the horizontal electric conductivity of thin cluster films over extensions of dozens of nanometres is below the detection limit,[11] whereas tunnelling processes between clusters over shorter distances (20 nm) have been observed.[12] Since the layers under investigation are of millimetre dimension, horizontal measurements seem unnecessary. However, the question whether

electron tunnelling between cluster layers that are separated from each other by SiO_2 films of varying thickness will be possible is of general interest.

Results and Discussion

Generation of Cluster/SiO_2 Multilayers

The aim of this work was to generate and electrically characterise multilayer systems as shown schematically in Figure 1 with varying numbers of layers.

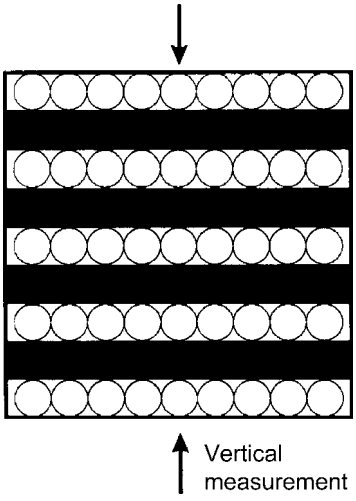

Figure 1. Sketch of a multilayered system consisting of nanoparticles and isolating barrier films.

The construction of the SiO_2 films was performed by plasma-assisted physical vapour deposition (PAPVD). The process is shown in Figure 2.

Figure 2a shows the relevant circuits of the system, and Figure 2b illustrates the process leading to the SiO_2 films. A piece of silicon in a carbon boat, which is linked to the anode, is positioned opposite the cathode, which consists of brass (1). The optimal pressure and the current conditions needed to generate 5 nm SiO_2 films were found to be 2×10^{-2} mbar O_2 and 75 A. After formation of a stable arc (2), the silicon begins to evaporate and moves towards the substrate (3). The jets of the cathode meet the silicon vapour and ionise it resulting in the anodic plasma (4). The anodic plasma expands into the vacuum reaching the substrate with the condensation of the silicon ions (5). Due to the presence of oxygen, SiO_2 is deposited (6). The stoichiometry is not perfect, and there may be a deficit of oxygen to a certain extent, but this should not influence the further steps. The time taken to produce a 5 nm SiO_2 film is only 3 s. As has been shown by the AFM investigations, the roughness of the as-prepared films is only 0.1 nm. Such surfaces are thus best suited for the generation of perfect cluster layers. Figure 3 shows a photograph of the whole apparatus.

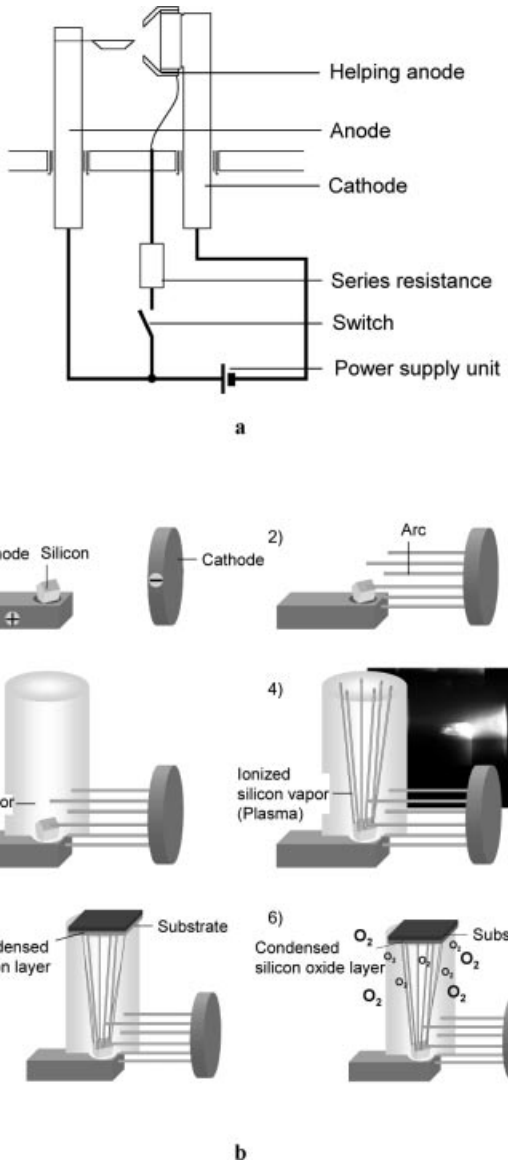

Figure 2. Illustration of the anodic plasma arc process. **a**: circuits for the PAPVD process, **b**: schematic drawing of the coating process using an anodic plasma arc.

To generate cluster double layers, diluted solutions of $Au_{55}(PPh_3)_{12}Cl_6$ clusters in dichloromethane (4.3×10^{-6} M) were used for spin coating. To cover a 1×1 cm^2 area, 50 μL are necessary, which are dropped onto a silicon wafer surface that is rotating at 100 revolutions per minute. After 5 s, the speed is accelerated to 4000 revolutions per minute, resulting in double layers, as can be seen from the AFM image in Figure 4.

The roughness was found to be 0.2 nm. The thickness of the film was determined by generating a cluster-free window by means of the AFM tip. The height profile is also shown in Figure 4. With a value of 5 nm, it agrees perfectly with a cluster double layer.

From the AFM sequences in Figure 5, it can be seen that the coating of the cluster layers with SiO_2 films occurs without destruction by the plasma process.

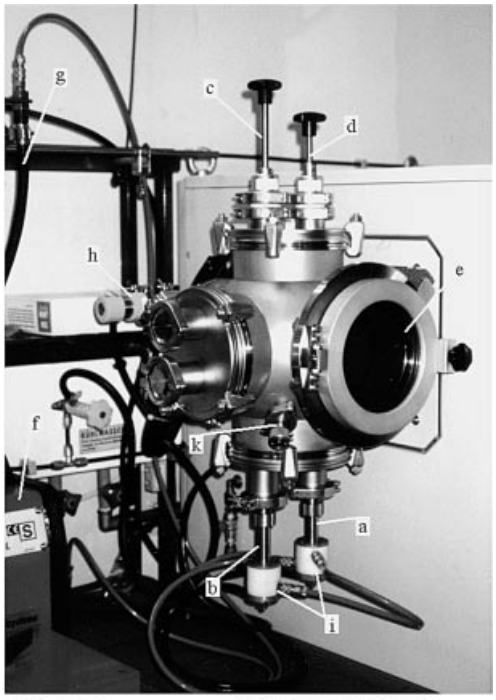

a) Cathode
b) Anode
c) Substrate fastener
d) Shutter
e) Inspection glass
f) Power supply unit
g) Series resistance
h) Needle valve
i) Water supply
k) Valve

Figure 3. Photograph of the whole apparatus for the PAPVD process.

Beginning with a silicon wafer (a), spin coating results in a cluster double layer (b). Coating with a 5-nm SiO_2 film (c) occurs and the surface structure is maintained. As a typical example, Figure 6 shows a transmission electron microscopy image (TEM) of a sectioned piece of a seven-layer system. For better visualisation, a sample with 15-nm SiO_2 layers has been selected. For later electric measurements, only 5 nm films will be considered, since the resistance of the 15 nm films was too high.

As can be seen, the parallel cluster layers consist of individual particles and are without visible defects. The final SiO_2 film still exhibits a low surface roughness of ca. 0.7 nm.

Side Effects

Before discussing the electric properties of multilayers, some side effects will briefly be considered: hydrodynamic instabilities of the cluster layers, and thermodynamic instabilities and optical properties of the multilayers.

The homogeneous coverage of the Si wafers or the SiO_2 films by $Au_{55}(PPh_3)_{12}Cl_6$ clusters from dichloromethane solutions is only possible with solvent that contains moisture (this can be achieved by contact of CH_2Cl_2 with air for a couple of days). The use of absolutely dry solvents results in an insufficient wettability of the wafer surface, actually consisting of a very thin SiO_2 film if handled in air. Absolutely dry solvents cause the Bénard–Marangoni effect.[13–18] This effect deals with the evaporation of thin liquid films

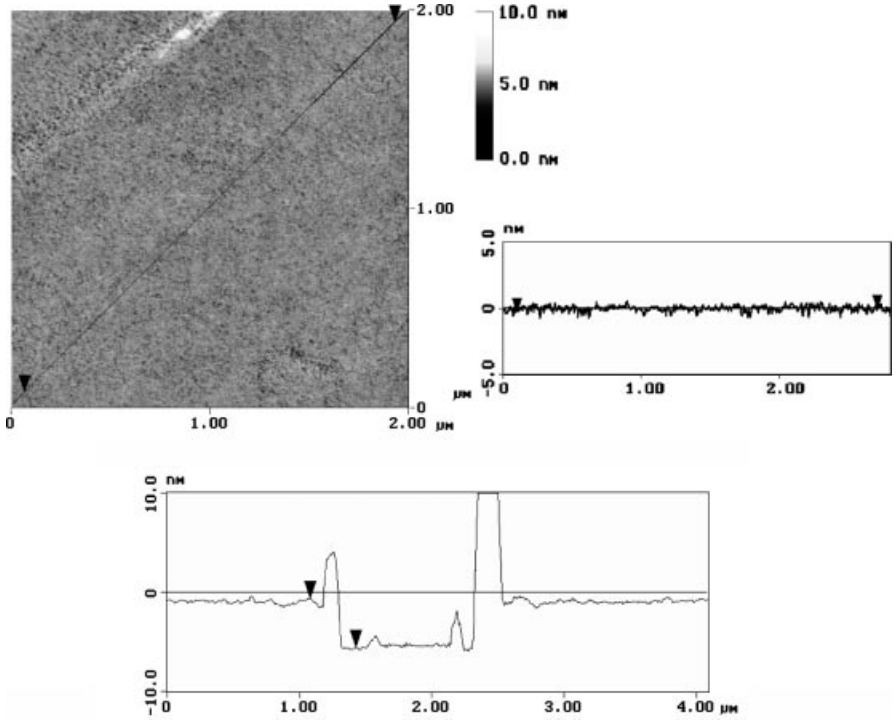

Figure 4. AFM image of a $Au_{55}(PPh_3)_{12}Cl_6$ double layer (left), roughness profile (0.2 nm) (right), and height profile (bottom) of 5 nm, generated by scratching a window into the layer with the AFM tip.

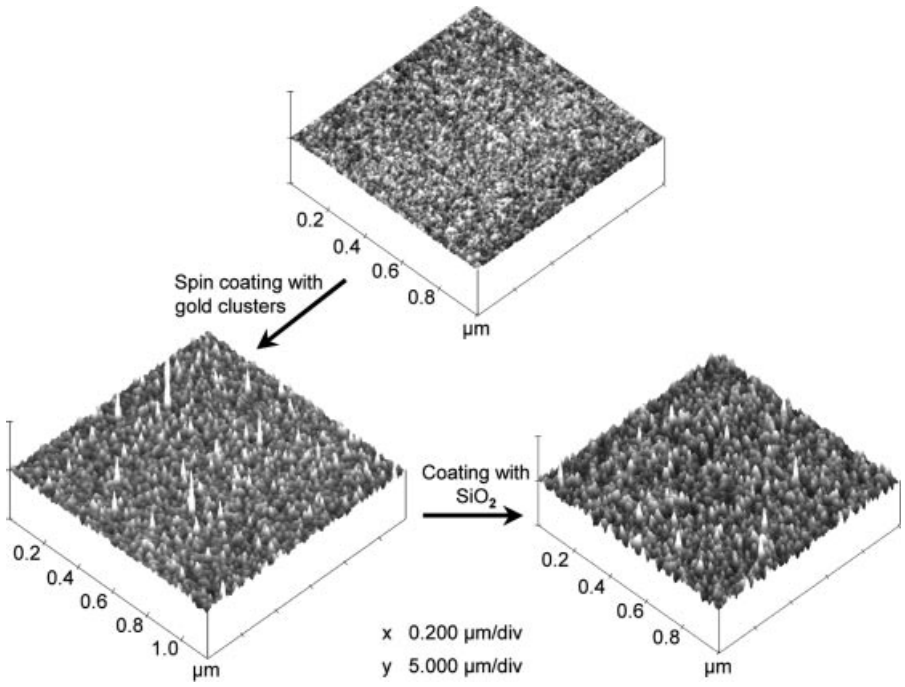

Figure 5. AFM images of a silicon wafer surface (top), a cluster double layer generated by spin coating (left) and a SiO_2 film on top of the cluster film (right), indicating that the SiO_2 does not destroy the cluster layer.

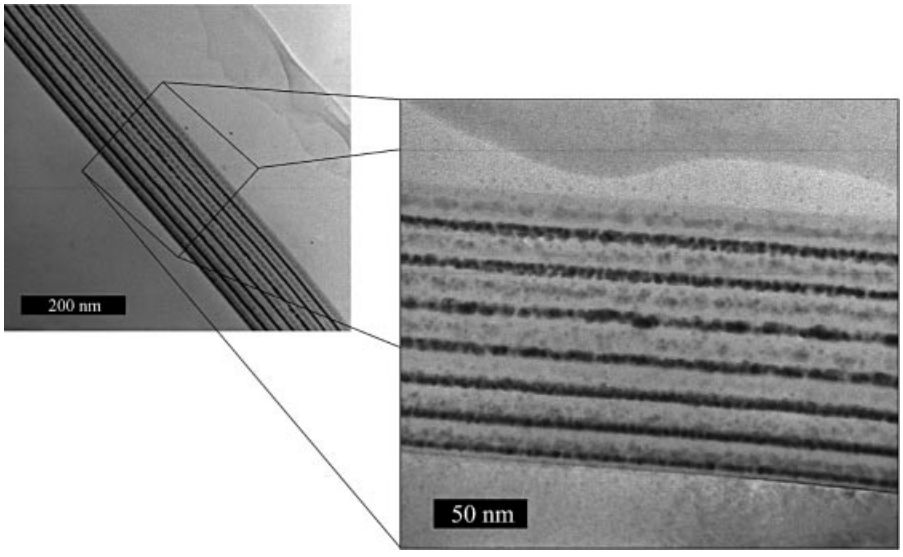

Figure 6. SEM image of a sectioned multilayer system consisting of seven cluster/SiO_2 combinations (black: cluster layers, grey: SiO_2 films).

on substrates. Hydrodynamic instabilities and surface tensions lead to diffusion processes from the warm substrate to the cooler liquid/air interface. A constant flow inside the liquid film is generated, which results in the formation of hexagonally oriented cells. At the borders of these cells, the particles, dissolved in the solvent, are deposited, and finally form hexagonal patterns. Figure 7 illustrates the Bénard–Marangoni effect, and Figure 8 shows light microscopy and scanning electron microscopy (SEM) images of some of the observed hexagonal patterns on glass (top) and on Si wafer (bottom), respectively.

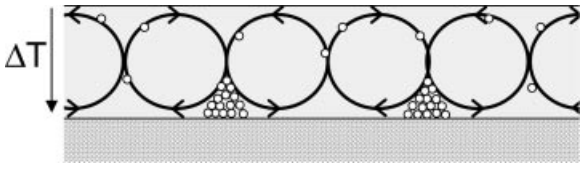

Figure 7. Illustration of the Bénard–Marangoni effect.

It should, however, be mentioned that the formation of such hexagonal structures is not expressed as much when spin-coating techniques are used, relative to simple addition

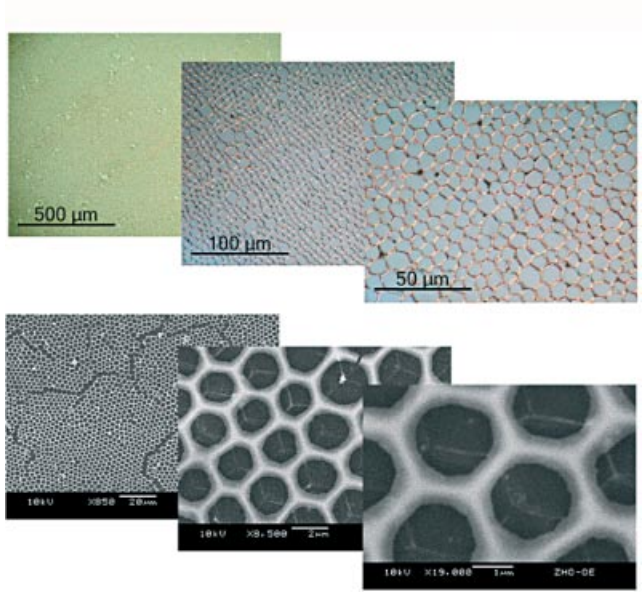

Figure 8. Light microscopy images (top) and SEM images (bottom) of the hexagonal patterns of $Au_{55}(PPh_3)_{12}Cl_6$ clusters on glass substrates (top) and on Si wafers (bottom), respectively. The structures form if the wetting conditions are not appropriate. Bars in the SEM images: 20 µm, 2 µm and 1 µm (from left).

of the cluster solution to the surface of a substrate. The concentrations of the solutions have little influence on the structure formation.

Another effect is observed that indicates the instability of the multilayers in the case of thicker SiO_2 interfaces. The SiO_2 films, generated by the discussed plasma process, are amorphous. In the cases of multilayers with SiO_2 films thicker than 15 nm, there is a tendency of the multilayer to spontaneously crystallise. This tendency is greater as the thickness of the SiO_2 films and the number of layers in-

Figure 9. Photograph of a crystallized multilayer sample.

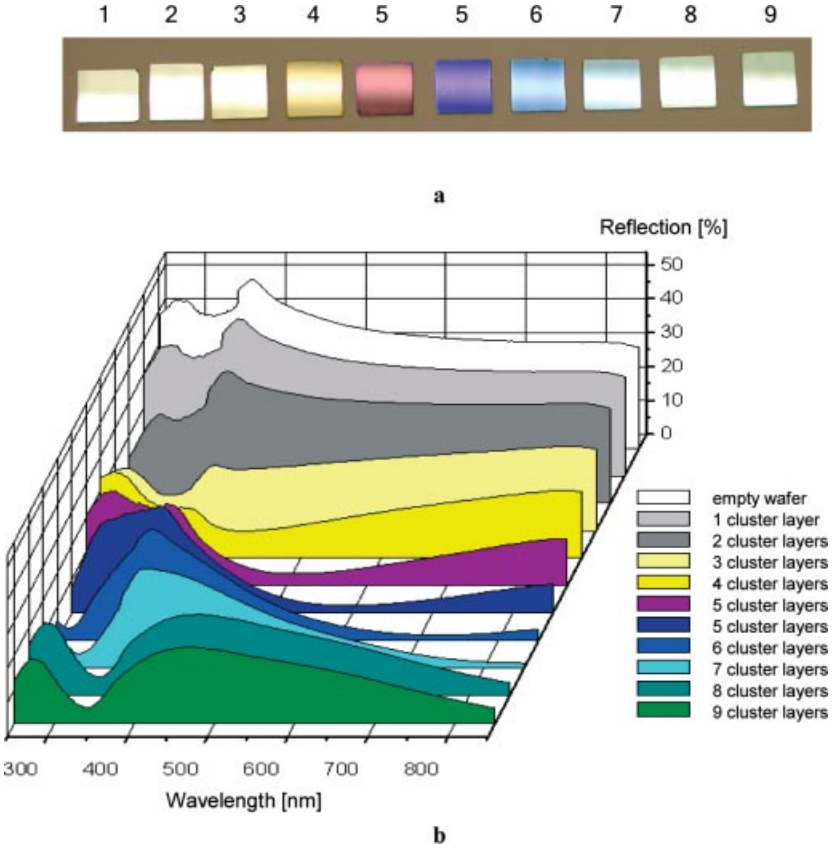

Figure 10. Changes in colour with increasing numbers of layers. **a**: photograph of multilayers consisting of 5-nm cluster layers and 30-nm SiO_2 films. **b**: UV/Vis spectra of the samples shown in **a**, measured in reflection.

crease. Figure 9 shows an optical image of a crystallised multilayer sample consisting of five cluster/SiO_2 combinations with 40-nm SiO_2 films. Three different types of crystallisation can be seen, macroscopically observable by different colours.

This phenomenon can be compared with the known metal-induced crystallisation of amorphous silicon.[19] Multilayers with SiO_2 intermediates that are <15 nm are stable with respect to crystallisation, whereas pure SiO_2 films that are even more than 15 nm thick are stable in the absence of gold clusters. This clearly indicates cluster-induced crystallisation.

A last phenomenon should be mentioned: the change in colour of the multilayers with increasing numbers of layers. As an example, the colour development and the UV/Vis spectra of a series of layered systems, consisting of cluster double layers and 30-nm SiO_2 films, are shown in Figure 10 (one to nine combinations).

It can be assumed that the reason for this observation is interference between the layers because of reflection and refraction. The fact that various numbers of SiO_2 films do not show any similar effects proves the influence of the gold cluster layers with a different refraction index in between.

Electrical Properties

For vertical measurements, the multilayer systems were contacted from the wafer side with conductive silver paint and from the top SiO_2 film by a gold contact that was made by evaporation of gold through a mask with a central hole with a diameter of 3 mm. As it turned out, reliable and reproducible current–voltage measurements were not possible with as-prepared multilayer systems. One of the reasons was the electrical behaviour of the silicon substrates, which masked the weak additional influence of the multilayers on top. Another reason was assumed to exist in the randomly oriented cluster double layers, which enabled the formation of differing individual conduction paths throughout the samples and therefore prevented reproducibility. In another paper involving this issue, we describe the investigation of multilayer systems with cluster monolayers and gold as a substrate. Thus, in this case perfect current–voltage measurements are possible.

The electric behaviour of the multilayers described in this contribution was investigated by capacitance measurements by means of complex impedance spectroscopy. Impedance spectroscopy (IS) is an experimental method for the analysis of charge carrier dynamics in an electrode/sample system. For this, an alternating electric field with a frequency range of 1–10^7 Hz is applied as an external perturbation of a system that is being tested under equilibrium conditions. By applying an electric field, local as well as translational charge carrier motion may be induced, which leads to the polarization of the sample. Thus, IS is a non-destructive method for the analysis of charge transport as well as of grain boundary and interface polarisation in a solid material. IS has been intensively applied to characterise three-dimensionally organized $Au_{55}(PPh_3)_{12}Cl_6$ clusters.[20–23] The results were very valuable, since for the first time it could be shown that these nanoparticles behave as quantum dots with extremely small capacities between each other allowing single electron transport between individual clusters.

From the impedance investigations of the above-mentioned multilayer systems, we expected information about their electrical capacitance which is dependent on the number of cluster/SiO_2 combinations. For detailed capacitance measurements, multilayers with 5-nm SiO_2 films and 5-nm $Au_{55}(PPh_3)_{12}Cl_6$ double layers have been selected because of the instability of thicker SiO_2 films (see above).

First, we studied the frequency dependence of the capacitance of 5-nm SiO_2 films relative to cluster-containing multilayers. The pure SiO_2 samples show a frequency independent capacitance at frequencies below 10^3 Hz (Figure 11). A dispersion region can be observed at higher fre-

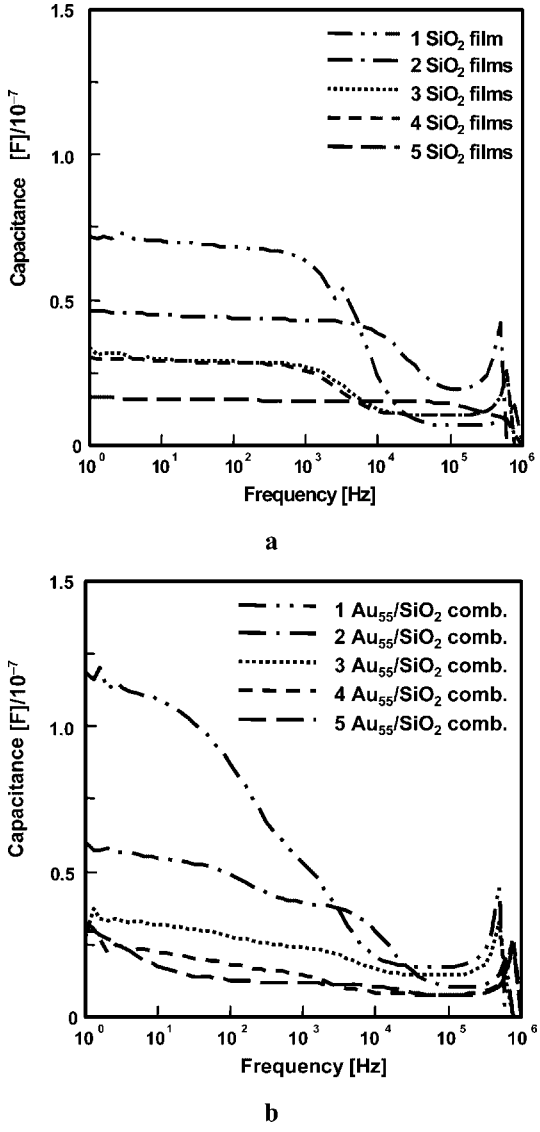

Figure 11. Frequency dependence of the capacitance in multilayered systems consisting of SiO_2 only (**a**) and of cluster/SiO_2 combinations (**b**).

quencies, where a decrease in the capacitance is observed. Additional peaks at 10^6 Hz are due to measurement artefacts. The cluster-containing samples show a similar behaviour, although higher capacitance values are observed. In samples 1, 2, and 5, an additional dispersion region at low frequencies can be recognised.

The geometry of the sample is an important factor for the experimentally determined capacitance values. In Figure 11, one can see that the capacitance of the samples decreases with increasing thickness of the layers. This is in agreement with the model of a parallel-plate capacitor with the capacitance $C = \varepsilon_r \times \varepsilon_0 \times A/d$, where C = capacitance, ε_r = relative permittivity of the system, ε_0 = permittivity of vacuum, A = square face of the system, and d = total thickness. The geometric effects can be eliminated by calculation of the relative permittivity ε_r of the sample being tested. Physically ε_r describes the transparency of matter in electric fields and, thus, is a measure of the polarisability. Figure 12 shows the relative permittivity of the samples plotted against the layer thickness for two different frequencies.

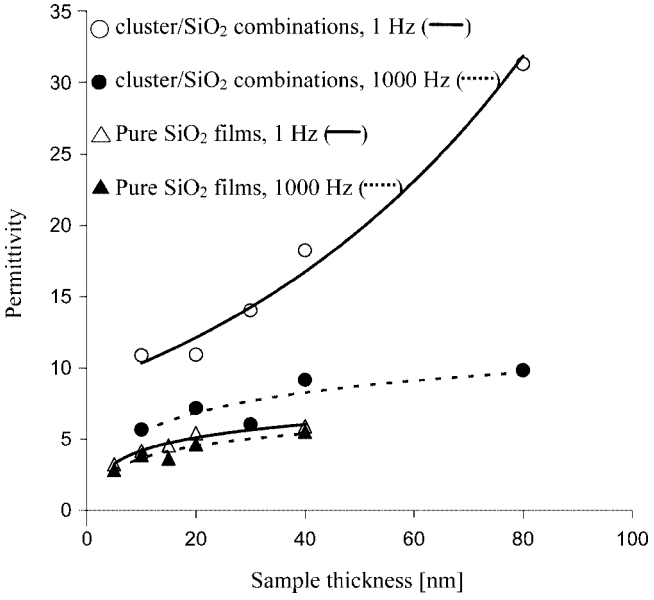

Figure 12. Illustration of the dependence of the relative sample permittivity on the sample thickness for two different measuring frequencies (The lines serve only as a guide for the eye).

It is clearly visible that the pure SiO_2 samples show a significantly smaller permittivity relative to the cluster-containing systems, and the permittivity only slightly increases with increasing layer thickness. The cluster/SiO_2 layer systems show increased permittivity with a pronounced progression as the number of the cluster layers increases. In all measurements, the permittivity at 1 Hz is larger than at 1 kHz, indicating that at low frequencies slow movement of charge carriers leads to an increase in the sample polarisation.

Samples without $Au_{55}(PPh_3)_{12}Cl_6$ clusters do not show significant changes in ε_r with increasing frequencies. Therefore, the increased polarisability of the multilayer systems must result from the presence of the cluster layers. We assign this phenomenon to the formation of dipoles in the cluster double layers and hence the formation of polarisation currents, as is indicated in Figure 13.

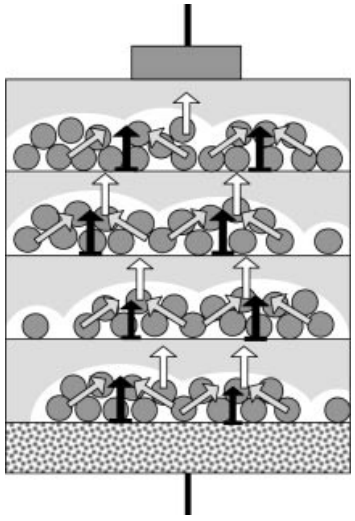

Figure 13. Illustration of the dipole formation in randomly oriented cluster double layers. Black and grey arrows indicate translational motion of charge carriers within the cluster layers parallel (black) to the applied electric field and disoriented (grey) with respect to the applied electric field. White arrows indicate the superposition of the local dipole moments forming a macroscopic dielectric polarisation.

Temperature-dependent capacitance measurements indicate a thermal activation of the polarisation processes in the cluster layers. In Figure 14, experimentally determined permittivity values at 1 Hz are plotted logarithmically versus the inverse temperature in an Arrhenius-like plot.

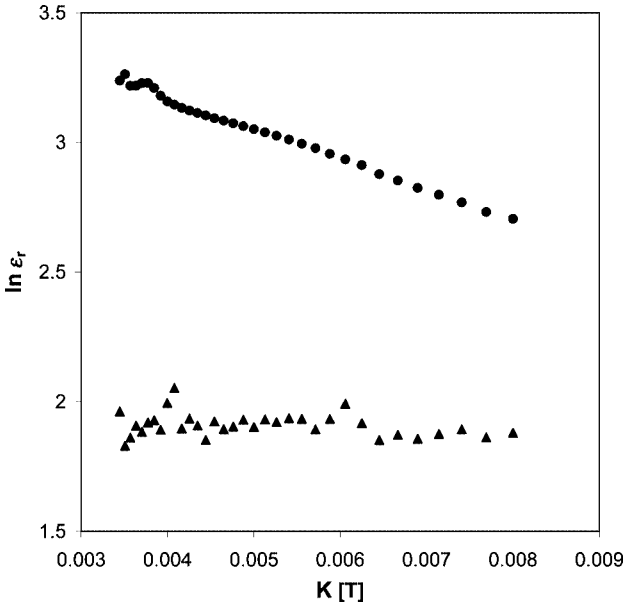

Figure 14. Arrhenius Plot of the temperature dependence of the capacitance for pure SiO_2 systems (triangles) and cluster/SiO_2 systems (dots).

The permittivity of pure SiO_2 samples is almost temperature independent, whereas cluster/SiO_2 systems show a temperature-dependent behaviour. For the latter structures an increase in the permittivity and therefore the number of polarization processes throughout the sample increases with increasing temperature.

Determination of the activation energy of the polarization processes in the sample by using the Arrhenius-relation gives a remarkably small value of 8.6 meV. However, this value is apparently lower than the activation energies determined for tunnelling processes between Au_{55} clusters, i.e. about 150 meV.[20–23] This might indicate that the polarisation process does not only reflect charge transport between the clusters within the layer, for which the activation energy measured was close to that of previous studies for pure cluster samples. We assume that additional local charge carrier transport occurs via defects in the oxide layer and/or at the interface between the clusters and SiO_2, which may exhibit smaller activation energies.

Conclusions

We have demonstrated the formation of multilayer systems, consisting of $Au_{55}(PPh_3)_{12}Cl_6$ double layers and SiO_2 barrier films of different thickness. The cluster double layer formation between the barrier films was performed by using spin-coating techniques, while the generation of the SiO_2 films resulted from a plasma assisted physical vapour deposition (PAPVD) process. Samples of up to nine cluster/SiO_2 combinations have been produced and have been characterised by AFM and SEM. Impedance measurements showed that there is a characteristic thermally activated frequency dependence of the capacitance of the different systems. The physical interpretation of this behaviour is the formation of dipoles in the non-ordered cluster double layers.

Experimental Section

Reagents and Physical Measurements: $Au_{55}(PPh_3)_{12}Cl_6$ was prepared as described.[24] Silicon wafers were used from SilChem, Freiberg, and consisted of n(As)-doped (111) silicon, 0.003 Ωcm, 375 μm. Silicon for SiO_2 layers: 99.999%, 0.2–1.5 mm, Balzers Materials, Liechtenstein. All solvents were reagent grade and used without further purification. CH_2Cl_2 for spin coating was kept in contact with air for 2–3 d in order to achieve the necessary water content. For optical imaging, a BX41 and a C3030 Zoom from Olympus, Hamburg, were used. AFM measurements were performed with a Nanoscope IIIa, Digital Instruments, Woodbury. SEM investigations were performed with a LEO 1530, LEO Elec-

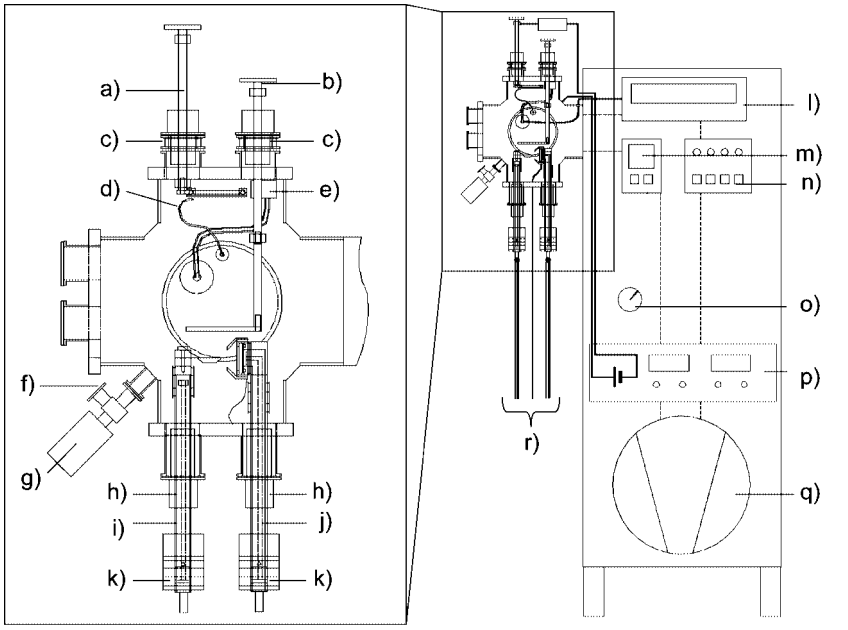

a) Substrate fastener
b) Shutter
c) Isolating lead-trough
d) Pipe for reactive gases
e) Quartz resonator device
f) Gas inlet
g) Needle valve
h) Isolating lead-trough
i) Anode with crucible
j) Cathode with helping anode
k) Water supply
l) Oscillating quartz crystal electronic
m) Pressure measurements
n) Vacuum control unit
o) Main switch
p) High voltage power supply
q) Vacuum pump
r) Electrical connection to power supply and computer-assisted measurements

Figure 15. Technical sketch of the PAPVD system with magnified recipient.

tron microscopy, Cambridge. For TEM investigations, a CM 200 FEG, Philips, Eindhoven, was used. For a spin coater, Model 6700, Speciality Coating Systems, Indianapolis, was used. The UV/Vis spectra were recorded with a Cary 1Bio, Varian, Palo Alto. The impedance measurements were performed with a Solartron (Farnborough) Impedance Analyzer SI 1260 in combination with a high-impedance input amplifier Solartron (Farnborough) 1296. For the low-temperature measurements, a cryostat of a Physical Property Measuring System by Quantum Design was used.

The device for the anodic plasma arc process was homemade, using commercially available building blocks, if possible. The technical principles behind were taken from patents[25–27] with permission and help from the patent owner Dr. H. Ehrich, Physics Department, University of Duisburg-Essen. A schematic overview over the whole device is shown in Figure 15. Details are also described in ref.[28].

Formation of SiO_2 films: The holder for the silicon was a self-made carbon boat. The silicon wafer was purified with ethanol and dried with a dust-off nozzle before it was fixed by glue 20 cm above the silicon container. The shutter is installed between sample and wafer. The recipient was evacuated to 5×10^{-5} mbar, and oxygen was then allowed to enter up to a pressure of 2×10^{-2} mbar. After reaching a constant pressure, the helping anode was linked with the power circuit. The power between the helping anode and cathode was then increased until a stable discharge between cathode and anode was reached; under the conditions to generate 5-nm SiO_2 films, it was 75 A. After having reached a stable discharge, the supporting anode was separated from the circuit and the shutter was opened. For the measurement of the thickness of the film, a quartz resonator device was used, however, only for films thicker than 10 nm since it is too slow to register thinner films in a few seconds. In those cases a coating parameter had to be determined over the time the sample is in contact with the ion flow. For the 5-nm layers, 3 s are necessary. Usually, the coating rate is 1–3 nm sec^{-1}. It can be adjusted by tuning the power strength and the gas inlet. The temperature in the sample during the coating process was 25–35 °C.

Spin Coating: In a typical spin-coating experiment a 1×1 cm^2 Si wafer was carefully cleaned with ethanol. After drying with a dust-off nozzle, the wafer was fixed on the sample holder of the spin coater by evacuation. Rotation with 100 revolutions per minute was started, and 50 μL of a 4.3×10^{-6} molar cluster solution was dropped on by means of a glass syringe. The whole surface should now be wet. The spin coater was then closed, and the speed was accelerated to 4000 revolutions per minute and kept there for 25 s. Each sample was controlled microscopically before further use. The multilayers were produced by alternative layers of SiO_2 films and the clusters.

Acknowledgments

This work was carried out as a project in the Schwerpunktprogramm 1072 of the Deutsche Forschungsgemeinschaft. We gratefully acknowledge this generous support.

[1] G. Schmid, R. Boese, R. Pfeil, F. Bandermann, S. Meyer, G. H. M. Calis, J. W. A. van der Velden, *Chem. Ber.* **1981**, *114*, 3634.
[2] L. F. Chi, M. Hartig, T. Drechsler, Th. Schwaak, C. Seidel, H. Fuchs, G. Schmid, *Appl. Phys. A* **1998**, *66*, 187.
[3] H. Zhang, G. Schmid, U. Hartmann, *Nanoletters* **2003**, *3*, 305.
[4] G. Schmid, R. Pugin, J.-O. Malm, J.-O. Bovin, *Eur. J. Inorg. Chem.***1998**, 813.
[5] G. Schmid, R. Pugin, W. Meyer-Zaika, U. Simon, *Eur. J. Inorg. Chem.***1999**, 2051.
[6] G. Schmid, M. Bäumle, N. Beyer, *Angew. Chem. Int. Ed.* **2000**, *39*, 181.
[7] G. Schmid, N. Beyer, *Eur. J. Inorg. Chem.* **2000**, 835.
[8] O. Vidoni, St. Neumeier, N. Bardou, J.-L. Pelouard, G. Schmid, *J. Cluster Sci.***2003**, *14*, 325.
[9] A. Vassiliev, H. Rehage, G. Schmid, St. Neumeier, W. Meyer-Zaika, *J. Cluster Sci.* in press.
[10] S. Liu, R. Maoz, G. Schmid, J. Sagiv, *Nanoletters* **2002**, *2*, 1055.
[11] G. Schmid, T. Reuter, St. Neumeier, unpublished results.
[12] Y. Liu, M. Schumann, T. Raschke, C. Radehaus, G. Schmid, *Nanoletters* **2001**, *8*, 405.
[13] P. Y. Su, J. C. Hu, S. l. Cheng, L. J. Chen, J. M. Liang, *Appl. Phys. Lett.* **2004**, *84*, 3480.
[14] V. V. Yaminki, K. Thuresson, B. W. Ninham, *Langmuir* **1999**, *15*, 3683.
[15] A. Oron, S. H. Daivs, S. G. Bankoff, *Rev. Mod. Phys.* **1997**, *69*, 931.
[16] P. C. Ohara, W. M. Gelbart, *Langmuir* **1998**, *14*, 3418.
[17] C. Stowell, B. Korgel, *Nanoletters* **2001**, *1*, 595.
[18] M. Maillard, L. Motte, M. P. Pileni, *Adv. Mater.* **2001**, *13*, 200.
[19] J. H. Kim, J. Y. Lee, *Jpn. J. Appl. Phys.* **1996**, *35*, 2052.
[20] U. Simon, G. Schmid, G. Schön, *Angew. Chem. Int. Ed. Engl.* **1993**, *32*, 250.
[21] G. Schön, U. Simon, *Coll. Polym. Sci.* **1995**, *273*, 101.
[22] U. Simon, *Adv. Mater.* **1998**, *10*, 1487.
[23] V. Torma, G. Schmid, U. Simon, *Chem. Phys. Chem.* **2001**, 5, 321.
[24] G. Schmid, *Inorg. Synth.* **1990**, *7*, 214.
[25] H. Ehrich, *EP 0015897281*, **1993.**
[26] H. Ehrich, *EP 0062086881*, **1995.**
[27] H. Ehrich, B. Hasse, H. P. Hinz, M. Mausbach, *EP* 0056660681, **1995.**
[28] T. Reuter, Ph.D. Dissertation, Universität Duisburg-Essen, **2004**.

Received: April 29, 2005
Published Online: July 20, 2005

